Journal of Alloys and Compounds 525 (2012) 39–43

Contents lists available at SciVerse ScienceDirect

Journal of Alloys and Compounds

journal homepage: www.elsevier.com/locate/jallcom

# Spectroscopic properties of $Nd^{3+}$ in $MgAl_2O_4$ spinel nanocrystals

P.J. Dereń*, K. Maleszka-Bagińska, P. Głuchowski, M.A. Małecka

*Institute of Low Temperature and Structure Research, Polish Academy of Sciences, ul.Okólna 2, 50-422 Wrocław, Poland*

ARTICLE INFO

*Article history:*
Received 25 November 2011
Received in revised form 2 February 2012
Accepted 6 February 2012
Available online xxx

*Keywords:*
Nanocrystallite
$MgAl_2O_4$ spinel
$Nd^{3+}$
Cross-relaxation
Sol–gel process

ABSTRACT

$Nd^{3+}$ doped $MgAl_2O_4$ spinel nanocrystals have been prepared by the sol–gel method. Their size decreases from 12 to 7 nm with increasing $Nd^{3+}$ concentration from 0.1 to 5%, respectively. Some crystal field components of the $Nd^{3+}$ energy levels in $MgAl_2O_4$ spinel were found from the 300 K reflectance absorption and the 77 K emission spectra. The $^4F_{3/2} \rightarrow {}^4I_{9/2}$ transition dominates in the emission spectra and accordingly spectroscopic-quality parameter (SQP) is equal to 3.3 for all samples. Decay time of the emission from the $^4F_{3/2}$ level in $MgAl_2O_4$:$Nd^{3+}$ (0.1%) nanocrystals is equal to 90 μs, and decreases with increasing neodymium concentration due to very efficient cross-relaxations. The slope of cross-relaxation rate is close to 2 which indicates fast donor–donor transfer.



## 1. Introduction

It was shown that change of the crystallites size from bulk to nano often results in new structural, electronic, and spectroscopic properties [1], therefore rare-earth activated nanomaterials are nowadays investigated extensively. One of the potential applications of these nanomaterials are phosphors in plasma display devices (PDP), field emission displays (FED), cathode ray tubes.

Magnesium aluminate belongs to wide spinel family. $MgAl_2O_4$ has the cubic crystal system with space group Fd3m [2,3]. In normal spinel $Mg^{2+}$ ion occupy tetrahedral sites and $Al^{3+}$ octahedral ones. Nanosized $MgAl_2O_4$ spinel was synthesized by several methods [4–7]. Magnesium spinel was doped with $Cr^{3+}$, $Co^{2+}$, and $Ti^{3+}$ [8–10]. The effect of $Tb^{3+}$ doping on the structure and spectroscopic properties in nanosized $MgAl_2O_4$ was investigated recently [11].

In this study we presented the results of synthesis of magnesium aluminate spinels doped with neodymium and their luminescent properties. It was assumed that $Nd^{3+}$ ions are substituted for $Mg^{2+}$ ions in $MgAl_2O_4$. Mismatch of valence and size of the replaced ions is manifested by broad excitation and emission bands. Influence of dopant concentration on spectroscopic properties was also investigated.

### 2. Experimental

Samples with varied neodymium concentration (0.1%, 0.5%, 1.0%, 2%, 5%) were prepared by modified Pechini's method [12]. As the starting materials $Mg(CH_3COOH)_2{\cdot}4H_2O$ (Alfa Aesar 99.99%), $AlCl_3{\cdot}6H_2O$ (Alfa Aesar 99.99%), and $Nd_2O_3$ were chosen. Citric acid and ethylene glycol were added as a chelating and polymerization agents, respectively.

Stoichiometric amounts of substrates were dissolved in deionized water. $Nd_2O_3$ was dissolved in dilute $HNO_3$ to transfer them into soluble in water nitrate salt and the excess of acid was evaporated at high temperature. Afterwards all substrates were dissolved in deionized water and mixed with the solution of ethylene glycol and citric acid. The fixed molar ratio of citric acid and ethylene glycol to total chelated metal cations was 5:1. After that final homogeneous solution was placed into plastic containers and kept into dryer at 80 °C until brown resin was obtained. Subsequently above resin was sintered at 900 °C for 3 h in air atmosphere with 15 °C/min temperature rise step. Structure and morphology studies of the obtained nanocrystallite powder were characterized using XRD powder diffraction and TEM microscopy.

The XRD patterns were measured using powder diffraction method on Panalitycal X'pert equipped with Cu Kα lamp. As a continuous excitation source 808 nm laser diode was used. Pulse excitation source was provided by second harmonic (532 nm) of Nd:YAG laser line. As a detector InGaAs diode was used. Emission spectra were measured on a McPherson spectrometer equipped with 150 W Xe lamp. Emission spectra were corrected for spectrophotometer sensitivity. To measure decay profiles we used digital oscilloscope LeCroy WaveSurfer 400.

## 3. Results and discussion

The XRD spectra (see Fig. 1) confirm that obtained powders are pure phase of $MgAl_2O_4$. Samples were annealed for short time, only 3 h and that makes an opportunity to receive nanocrystallites with an average grain sizes about 11 nm which was estimated using Scherrer's formula [13]. With increasing $Nd^{3+}$ content the lines in the XRD spectrum become broader, which is due to decreasing of the mean nanocrystallite size from 12 to 7 nm for 0.1 and 5% of $Nd^{3+}$, respectively.

Morphology of nanopowders was characterized with Transmission Electron Microscopy (TEM). TEM images are presented in Fig. 2. This investigation revealed range of grains size from 2 to 20 nm for

* Corresponding author.
*E-mail address:* P.Deren@int.pan.wroc.pl (P.J. Dereń).

0925-8388/$ – see front matter © 2012 Elsevier B.V. All rights reserved.
doi:10.1016/j.jallcom.2012.02.065

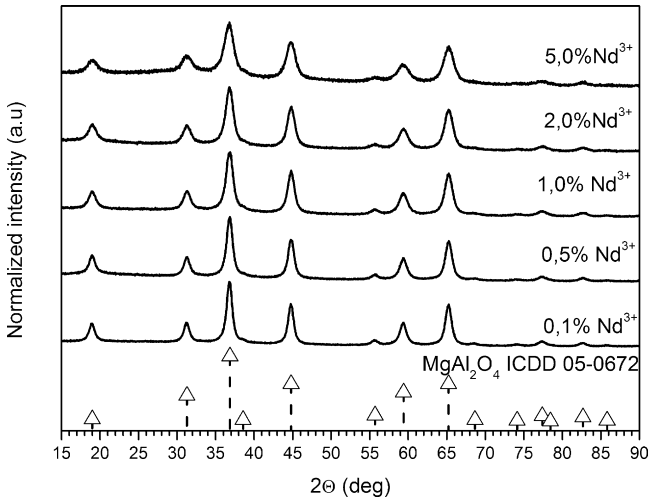


**Fig. 1.** XRD patterns of $MgAl_2O_4$:$Nd^{3+}$.

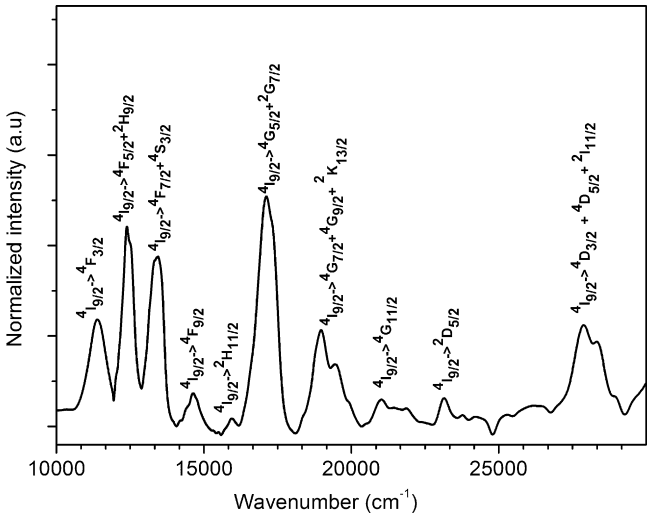


**Fig. 3.** Reflectance absorption spectra of $MgAl_2O_4$:1% $Nd^{3+}$ measured at 300 K.

the sample with the lowest concentration of neodymium (0.1%). When $Nd^{3+}$ content increases then growing of nanograins is inhibited and therefore for the sample with 5% of $Nd^{3+}$ the mean grain size ranges from 4 to 12 nm. Distribution of the nanocrystallite diameter decreases with increasing $Nd^{3+}$ concentrations. Inhibition of the crystals' growth is associated with crystallization process which depends on amount of dopant dissolved in a host lattice. This phenomenon was observed already by other authors [14].

Reflectance absorption spectra of $MgAl_2O_4$:$Nd^{3+}$ (5%) (see Fig. 3) were measured at room temperature. Characteristic bands for neodymium(III) ions are observed, the most intense is the $^4I_{9/2} \rightarrow {}^4G_{5/2}$ hypersensitive transition associated with the lanthanide's ion surrounding [15]. Second intense band centered at 803 nm (12 450 $cm^{-1}$) assigned the $^4I_{9/2} \rightarrow {}^4F_{5/2}$ transition is broad. Its full width at half its maximum intensity (FWHM) is equal to 450 $cm^{-1}$. It is useful feature because the energy of this band will match energy of wide range of laser diodes and thermal drift of the output diode emission wavelength will not affect pumping significantly. The reflectance absorption spectra and low temperature emission spectra allowed to obtain $Nd^{3+}$ energy levels in $MgAl_2O_4$ spinel, they are listed in Table 1. The spitting of the $^4F_{3/2}$ level is equal to 210 $cm^{-1}$, this rather high value is due to low symmetry of the $Nd^{3+}$ site. Similar values were observed in many other hosts like for example in: $NaGdGeO_4$ for which $\Delta E = 215\ cm^{-1}$ or $La_2Be_2O_5$; $\Delta E = 215\ cm^{-1}$ [15].

The emission spectra were measured at room temperature (see Fig. 4) and at 77 K (see Fig. 5). At 77 K the emission goes only from the lowest component of the $^4F_{3/2}$ level, therefore it was possible to distinguish transitions to the crystal field components of the $^4I_J$ therm. Three characteristic bands centered at 896, 1074, and 1352 nm are observed. They are due to transitions from the $^4F_{3/2}$ level to the ground, first, and second excited levels, the $^4I_{9/2}$, $^4I_{11/2}$, and the $^4I_{13/2}$, respectively. Transition to the ground $^4I_{9/2}$ level dominates the emission spectra. The $^4F_{9/2} \rightarrow {}^4I_{11/2}$ transition has almost the same intensity, third band is much less intense (see Fig. 4), the $^4F_{9/2} \rightarrow {}^4I_{15/2}$ transition was not observed in our setup.

Increased $Nd^{3+}$ concentration changes the emission spectra, the most significant changes are observed for spectra recorded at 77 K (see Fig. 5). With increasing the $Nd^{3+}$ concentration from 0.1 to 5% all lines become broader and exhibit red shift of 6 $cm^{-1}$. For 0.1% of $Nd^{3+}$ the most intensive peak in all bands is due to transition to the ground component of the $^4I_{9/2}$ level. Comparing the integrated intensity of this most intense peak to the integrated intensity of the

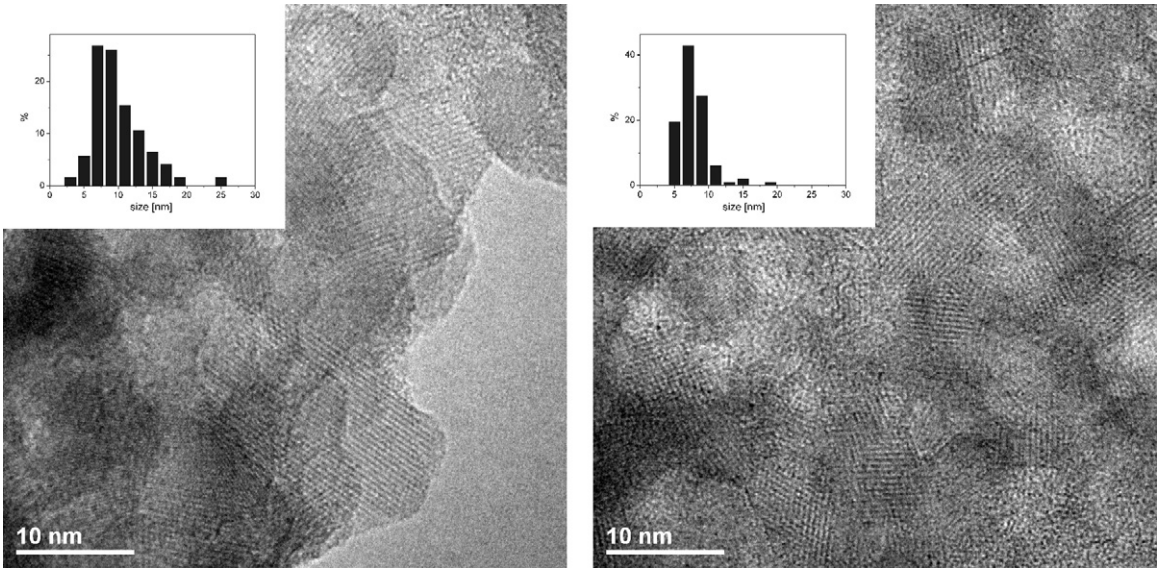


**Fig. 2.** TEM images of $MgAl_2O_4$:$Nd^{3+}$ (sample 0.1% on left and sample 5.0% on right side) prepared by the Pechini method.

**Table 1**
Energy levels and its Stark components found from the 300 K reflectance absorption and the 77 K emission spectra of nanocrystallite $MgAl_2O_4:Nd^{3+}$.

| Energy level of $Nd^{3+}$ | Energy ($cm^{-1}$) | $\Delta E$ ($cm^{-1}$) | Number of levels | |
|---|---|---|---|---|
| | | | Theoretical | Experimental |
| $^4I_{9/2}$ [a] | 0, 71, 175, 336, 483 [a] | 483 | 5 | 5 |
| $^4I_{11/2}$ [a] | 1958, 2099, 2234 [a] | 276 | 6 | 3 |
| $^4I_{13/2}$ [a] | 3911, 4005, 4068, 4242 [a] | 331 | 7 | 4 |
| $^4I_{15/2}$ [a] | 5835, 6134, 6350, 6625 [a] | 790 | 8 | 4 |
| $^4F_{3/2}$ [a,b] | 11 389 [a,b], 11 599 [a,b] | 210 | 2 | 2 |
| $^4F_{5/2} + {}^4H_{9/2}$ [b] | 12 023, 12 386, 12 523 [b] | 694 | 7 | 3 |
| $^4F_{7/2} + {}^4S_{3/2}$ [b] | 13 324, 13 555 [b] | 231 | 6 | 2 |
| $^4F_{9/2}$ [b] | 14 652 [b] | – | 5 | 1 |
| $^2H_{11/2}$ [b] | 15 966 [b] | – | 6 | 1 |
| $^4G_{5/2} + {}^2G_{7/2}$ [b] | 16 669, 17 179 [b] | 510 | 7 | 2 |
| $^4G_{7/2} + {}^4G_{9/2} + {}^2K_{13/2}$ [b] | 18 957, 19 531, 19 904 [b] | 947 | 16 | 3 |
| $^4G_{11/2}$ [b] | 20 990, 21 696 [b] | 706 | 6 | 2 |
| $^2D_{5/2}$ [b] | 23 153, 23 781 [b] | 628 | 3 | 2 |
| $^4D_{3/2} + {}^4D_{5/2} + {}^2I_{11/2}$ [b] | 27 909, 28 457 [b] | 548 | 11 | 2 |

[a] Data collected from the emission spectra measured at 77 K.
[b] Data collected from the reflectance absorption spectra measured at 300 K.

remaining part of the $^4F_{3/2} \rightarrow {}^4I_{9/2}$ band one can notice that the latter increases with $Nd^{3+}$ concentration and is 1.8 times more intense for 5% of $Nd^{3+}$ than for 0.1% sample. The full width at half maximum also increases with concentration from 631 for 0.1% to 691 $cm^{-1}$ for 5% of dopant. This observation is in general valid for all emission bands. The transition intensity to the lower crystal field component decreases and the emission bands are broader with increasing $Nd^{3+}$ concentration.

It indicates that $Nd^{3+}$ ions are located in many non-equivalent positions in $MgAl_2O_4$ nanocrystals. The number of so many "sites" is created by the sample morphology. It is evident that volume to surface ratio is small in nanocrystals comparing to bulk materials. Taking the magnesium spinel lattice constant as the thickness of sample surface one can easily calculate that for the samples doped with 5% $Nd^{3+}$ (nanocrystallite diameter equal 7 nm) almost 1/3 of spinel cells are located on the surface, while for the 0.1% of $Nd^{3+}$ (nanocrystallite diameter equal 12 nm) only 1/5. Neodymium ions located in "surface unit cells" see another surroundings than ions inside the crystallite. Since with increased neodymium concentration crystallite size decreased more $Nd^{3+}$ ions are located on the surface. Valence mismatch between $Mg^{2+}$ and $Nd^{3+}$ and difference in their size, 86 and 112 pm, respectively, creates additional defects like vacancies or inversion of spinel structure [3]. As a consequence with increasing dopant concentration stronger broadening is observed in the emission spectra.

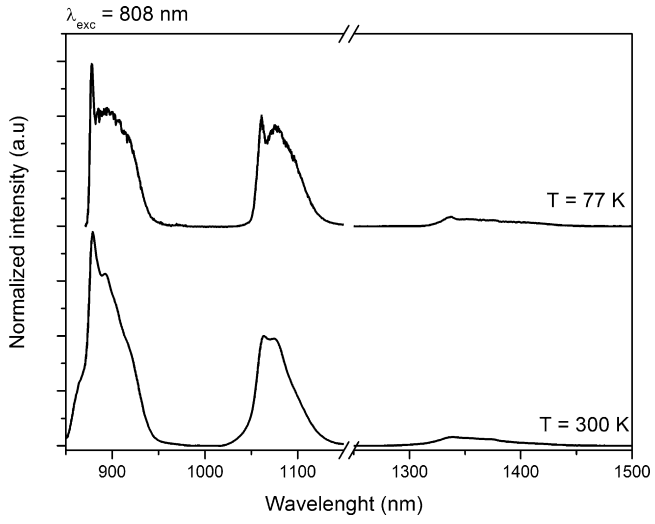


**Fig. 4.** Emission spectra of $MgAl_2O_4:Nd^{3+}$ excited by $\lambda_{exc}$ = 808 nm, measured at 300 K and 77 K for 1% of $Nd^{3+}$.

Since the spectra were corrected for the sensitivity of the spectrophotometer we could calculate so called spectroscopic quality parameter (SQP) $\chi_{Nd}$ (where $Y_{Nd} = {}^4I_{11/2}/{}^4I_{13/2}$ and $I_J$ are integrated intensities of the relevant emission bands), SQP was calculated using below equation [15]:

$$\chi_{Nd} = 0.765 Y_{Nd} - 2.96 \quad (1)$$

$\chi_{Nd}$ by definition is equal to $\Omega_4/\Omega_6$ ratio, where $\Omega_\lambda$ are Judd–Ofelt intensity parameters [16,17]. It has values greater than 3, which was reported only for few crystals. According to graph of branching ratio presented by Kaminski [15] such high value is

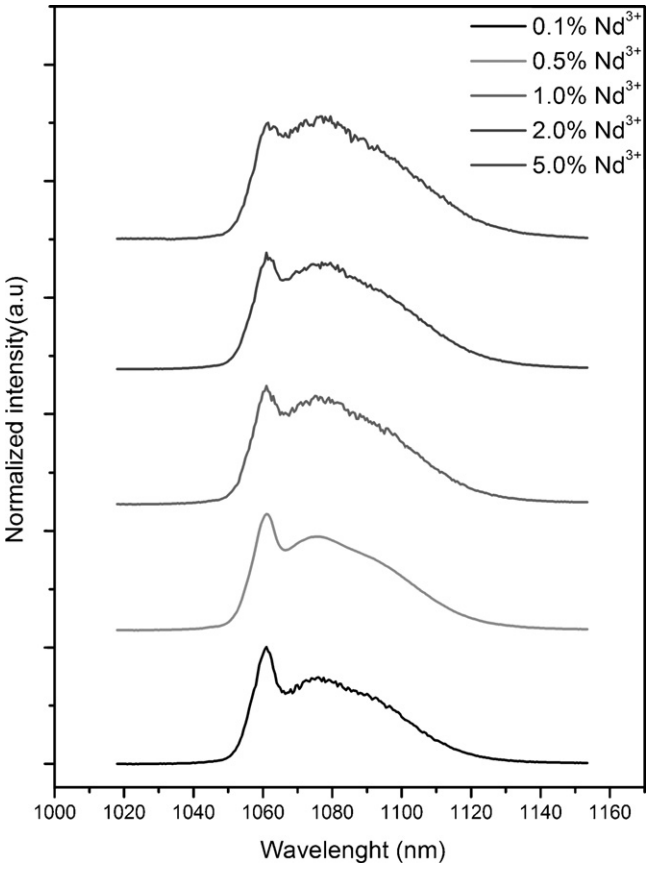


**Fig. 5.** The $^4F_{3/2} \rightarrow {}^4I_{11/2}$ transition of $MgAl_2O_4:Nd^{3+}$ excited by $\lambda_{exc}$ = 808 nm, measured at 77 K in function of neodymium(III) concentration.

**Table 2**
Spectroscopic-quality parameter values obtained from the emission spectra of nanocrystalline $MgAl_2O_4$:$Nd^{3+}$ recorded at 300 K.

| Concentration of $Nd^{3+}$ (%) | SQP |
|---|---|
| 0.1 | 3.34 |
| 0.5 | 3.02 |
| 1.0 | 3.34 |
| 2.0 | 3.32 |
| 5.0 | 3.32 |

typical for the host when the $^4F_{3/2} \rightarrow {}^4I_{9/2}$ is the most intense transition. Indeed the first band either at room and 77 K is the strongest one. We have to stress also that Judd–Ofelt intensity parameters are host depended and do not depend on concentration. In $MgAl_2O_4$:$Nd^{3+}$ the $\chi_{Nd}$ changes slightly from sample to sample (see Table 2) and these changes are so small that could be assigned to experimental error. Therefore, one may conclude that neodymium concentration in the range 0.1–5% do not change properties of the $MgAl_2O_4$ host.

The luminescence decay profiles of the $^4F_{3/2}$ emission were recorded at 877 nm. They have multiexponential character, which is seen especially for the sample with 5% of $Nd^{3+}$ (see Fig. 6) and decay time was calculated as

$$\tau = \int \frac{I(t)dt}{I_0}. \quad (2)$$

For 77 K decay times are shorter than at room temperature. Decrease of the lifetime with temperature decreasing was also observed by the other authors [18–20]. They explained this phenomenon by taking into account decay time of the second component of the $^4F_{3/2}$ level. At 77 K the higher component is no more populated and we can measure decay constant of only lower one. Consequently lifetime of the $^4F_{3/2}$ levels at 300 K is described by the following equation:

$$\tau_{rad} = \frac{1 + e^{-\Delta E/kT}}{(1/\tau_1) + (1/\tau_2)e^{-\Delta E/kT}} \quad (3)$$

where $\tau_1$ and $\tau_2$ are the lifetime of lower and upper crystal field components of the $^4F_{3/2}$ level. Energy separation between them is $\Delta E = 210\,cm^{-1}$ (see Table 1). For calculation we took for $\tau_1$ decay time measured at 77 K. The estimated from Eq. (3) lifetime $\tau_2$ is equal 340 μs, which is quite similar to values obtained by the other authors [18–20]. The calculations were done for sample with the lowest concentration of neodymium, to avoid the errors introduced by the concentration quenching processes.

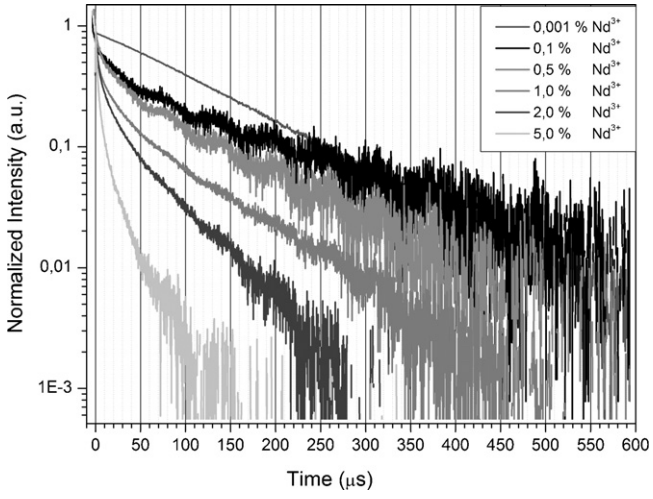


**Fig. 6.** Decay profiles of the $^4F_{3/2}$ emission of $Nd^{3+}$ ions in $MgAl_2O_4$ measured at 300 K.

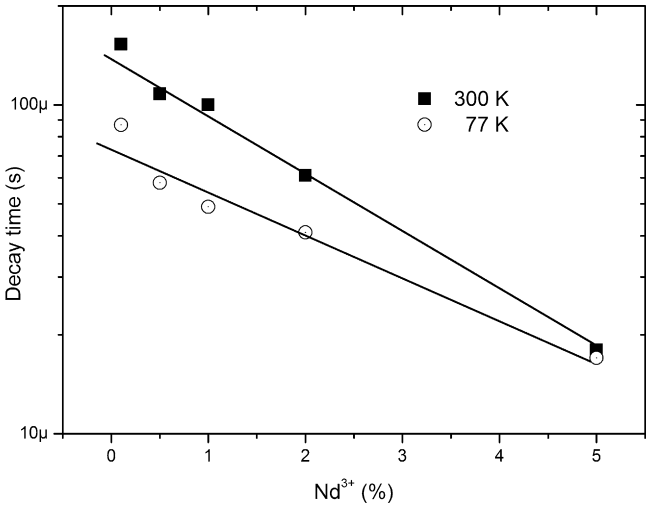


**Fig. 7.** Decay time of the $^4F_{3/2}$ emission of $Nd^{3+}$ ions in $MgAl_2O_4$ in function of neodymium concentration measured at room and liquid nitrogen temperature. The lines serve to guide the eyes.

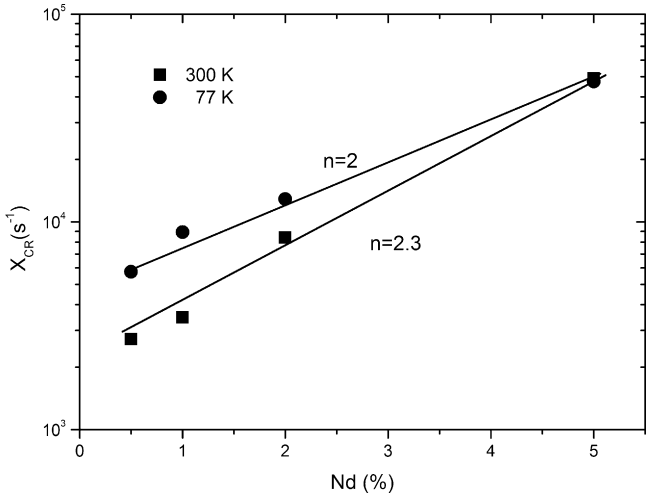


**Fig. 8.** Cross relaxation rate of the $^4F_{3/2}$ level at liquid nitrogen and room temperature in function of $Nd^{3+}$ concentration in the $MgAl_2O_4$ spinel lattice.

Decay times of the $^4F_{3/2}$ emission decrease with increasing $Nd^{3+}$ concentration (see Fig. 7) because nonradiative transitions increase. The shortening of decay time is significant and for 5% $Nd^{3+}$ decay time has only 12% of its value registered for 0.1%. We have measured decay time of the sample doped only with 0.001% of $Nd^{3+}$. The decay profile at 300 K is single exponential (see Fig. 6) and decay time is equal to 150 μs, it is the same value calculated applying Eq. (2) for the 0.1% sample.

Since energy gap between the $^4F_{3/2}$ and $^4I_J$ manifold is large, multiphonon nonradiative transitions could be neglected in this host. One can argue that in such small nanoparticle effective surface is large and adsorb gases, which may quench emission, but in function of concentration the main factor which makes emission shorter is cross-relaxation (CR). There are several possibilities of almost resonant CR, for example:

$(^4F_{3/2}, {}^4F_{3/2}) \rightarrow (^4I_{11/2}, {}^4G_{11/2})$
$(^4F_{3/2}, {}^4F_{3/2}) \rightarrow (^4I_{13/2}, (^4G_{7/2} + {}^4G_{9/2} + {}^2K_{13/2}))$
$(^4F_{3/2}, {}^4F_{3/2}) \rightarrow (^4I_{15/2}, (^4G_{5/2} + {}^2G_{7/2}))$
$(^4F_{3/2}, {}^4I_{9/2}) \rightarrow (^4I_{15/2}, {}^4I_{15/2})$

This type of rapid donor–donor transfer was described by Huber [21,22]. Characteristic feature for such transfer is well manifested in decay profile, which at its beginning is multiexponential and at its end become single exponential (see Fig. 6).

With increasing of $Nd^{3+}$ concentration the number of $Nd^{3+}$–$Nd^{3+}$ pairs increases. The cross-relaxation $X_{CR}$ rate was calculated using the below equation [23]:

$$X_{CR} = \frac{1}{\tau} - \frac{1}{\tau_0} \quad (4)$$

where $\tau$ is the luminescence decay time, $\tau_0$ lifetime measured for the sample with the lowest neodymium concentration. The slope of CR transfer rate is close to 2 (see Fig. 8). Stronger, $n = 2$, 3 CR rate is observed at room temperature, because cross-relaxation is phonon assisted and therefore more effective.

## 4. Conclusion

Synthesis of $MgAl_2O_4$ nanocrystallites doped with different $Nd^{3+}$ concentration in the range 0.1–5% was developed. Nanocrystallites were pure-phase magnesium spinel. The nanocrystallites mean size decreases from 12 to 7 nm with increasing $Nd^{3+}$ concentration from 0.1 to 5%, respectively. For all samples the $^4F_{3/2} \rightarrow {}^4I_{9/2}$ transition is the most intense in the emission spectra. It is well correlated with spectroscopic quality factor equal to 3.3, which remains the same in the $Nd^{3+}$ concentration range equal to 0.1–5%. It indicates that dopant do not changes host properties up to 5%. Emission intensity as well as decay times of higher doped samples are affected by cross-relaxation processes which are very effective.

## Acknowledgment

This work was financially supported by the Ministry of Science and Higher Education under Grant no. N N507 372335, which is greatly acknowledged.

## References

[1] C.N. Rao, A. Muller, A.K. Cheetman, The Chemistry of Nanomaterials, Wiley-VCH Verlag, 2004, pp. 3–4.
[2] K.E. Sickafus, J.M. Will, J. Am. Ceram. Soc. 82 (1999) 3279.
[3] H.K. Muller-Buschbaum, J. Alloys Compd. 349 (2003) 49–104.
[4] J. Omkaram, G. Seeta Rama, S. Raju, S. Buddhudu, J. Phys. Chem. Solids 69 (2008) 2066–2069.
[5] R.J. Wiglusz, T. Grzyb, S. Lis, W. Stręk, J. Lumin. 130 (2010) 434–441.
[6] J.G. Li, T. Ikegami, J-H. Lee, T. Mori, Y. Yajima, J. Eur. Ceram. Soc. 21 (2001) 139–148.
[7] E.N. Alvar, M. Rezaei, H.N. Alvar, Powder Technol. 198 (2010) 275–278.
[8] P.J. Deren, M. Malinowski, W. Strek, J. Lumin. 68 (1996) 91–103.
[9] P.J. Dereń, W. Stręk, U. Oetliker, H.U. Güdel, Phys. Status Solid. 182 (1994) 241–251.
[10] L.E. Bausá, I. Vergara, J. García-Solé, W. Strek, P.J. Dereń, J. Appl. Phys. 68 (1990) 736–740.
[11] R.J. Wiglusz, T. Grzyb, Opt. Mater. 33 (2011) 1506–1513.
[12] M.P. Pechini, US Patent 3330 (1967) 697.
[13] P. Scherrer, Nachr. Ges. Wiss. Göttingen 2 (1918) 96–100.
[14] M.A. Małecka, U. Burkhardt, D. Kaczorowski, M.P. Schmidt, D. Goran, L. Kępiński, J. Nanopart. Res. 11 (2009) 2113.
[15] A.A. Kaminskii, Crystalline Lasers: Physical Processes and Operating Schemes, CRC Press, New York, 1996, pp. 235–238.
[16] B.R. Judd, Phys. Rev. 127 (1962) 750.
[17] G.S. Ofelt, J. Chem. Phys. 37 (1962) 511.
[18] I. García-Rubio, J.A. Pardo, R.I. Merino, R. Cases, V.M. Orera, J. Lumin. 86 (2000) 147–153.
[19] P.J. Dereń, A. Bednarkiewicz, Ph. Goldner, O. Guillot-Noel, J. Appl. Phys. 103 (2008), 043102.
[20] K. Lemański, A. Gągor, M. Kurnatowska, R. Pązik, P.J. Dereń, J. Solid State Chem. 184 (2011) 2713–2718.
[21] D.L. Huber, in: W.M. Yen, R.M. Selzer (Eds.), Laser Spectroscopy of Solids, Springer-Verlag, Berlin, 1981, pp. 83–111.
[22] D.L. Huber, Phys. Rev. B 20 (1979) 2307–2314.
[23] M. Malinowski, M. Kaczkan, S. Turczyński, D. Pawlak, Opt. Mater. 33 (2011) 1004–1007.